Substrate-enhanced O_2 adsorption and complexity in the Raman *G*-band spectra of individual metallic carbon nanotubes

Anshu Gaur and Moonsub Shim*
Department of Materials Science and Engineering, University of Illinois at Urbana-Champaign, Urbana, Illinois 61801, USA
(Received 9 June 2008; published 29 September 2008)

The role of oxide substrate with respect to O_2 adsorption induced changes in the Raman spectra of individual metallic carbon nanotubes is examined. A chiral metallic nanotube suspended over a trench exhibits a relatively simple two-peak *G*-band feature with no observable *D*-band intensity. On the other hand, a much more complex Raman *G*-band feature along with significant *D*-band intensities are observed on the part of the nanotube resting on the oxide substrate. O_2 adsorption induced charge transfer and enhancement of physical disorder are considered to explain the differences observed. Spectral changes upon Ar annealing/O_2 exposure cycles on the on-substrate segment of a single nanotube are compared with those on the suspended part of the same nanotube. Complexity of the line shape and narrower linewidths are much more pronounced in the on-substrate part of the nanotube but continued annealing/O_2 adsorption cycle eventually leads to similar (but smaller) changes in the suspended part as well. Direct correlation between *D*-band intensity enhancements and the changes in the *G*–band (increasing complexity and the removal of phonon softening via the Kohn anomaly) suggest that O_2 adsorption not only causes charge transfer and physical disorder but also leads to otherwise not observable double-resonance *G*-band phonon modes to have significant intensities.

DOI: 10.1103/PhysRevB.78.125422 PACS number(s): 78.30.Na, 63.22.Gh, 78.67.Ch

I. INTRODUCTION

Resonance Raman spectroscopy is an important technique to characterize carbon nanotubes. In addition to chiral index (n,m) assignment,[1–4] Raman-scattering measurements can also be used to understand various physical and chemical processes from electron-phonon coupling[5–9] to chemical reactions[10–14] and charge transfer/doping[15–19] in single walled carbon nanotubes (SWNTs). SWNTs are extremely sensitive to the local chemical environment due to all atoms being at the surface and in particular O_2 adsorption on SWNTs and its effects on the observed electronic characteristics have been given much attention. However, most studies have been concerned with semiconducting SWNTs.[20–28] Less consideration has been given to O_2 adsorption on metallic SWNTs and its consequences. One of the debated issues of O_2 adsorption is its potential doping/charge-transfer effects. Such effects would be more pronounced in metallic SWNTs where there are available free electrons and electronic states at the Fermi level to participate in the charge-transfer process. We have previously shown that O_2 adsorption can indeed lead to changes in individual metallic nanotubes that are consistent with charge-transfer effect.[29] Namely, comparison between Raman *G*-band spectral changes under electrochemical gating with those induced by O_2 adsorption/desorption indicates that O_2 adsorption leads to a significant downshift of the Fermi level (i.e., electron removal) to several hundreds of meV below the Dirac point where the bands cross. Near this band crossing point, broadening and softening of *G*-band LO mode are expected to arise from the strong electron-phonon coupling due to the Kohn anomaly.[5,30–35] Hence this broad softened mode with an asymmetric Fano line shape has been attributed as intrinsic to single metallic nanotubes[29] without the need to invoke bundling effects.[36,37] The varying degree of O_2 adsorption causes variations in where the Fermi level lies with respect to the Dirac point and therefore variations in the degree of phonon softening and broadening.

Effects of O_2 adsorption are important to consider in understanding inherent properties of SWNTs. It is especially important in interpreting observed Raman *G*-band modes of metallic SWNTs where both charge transfer and physical disorder have been observed.[29] Hence a better understanding of the O_2 adsorption mechanism and the effects on Raman-scattering processes in metallic SWNTs is needed. Raman measurements at the single nanotube level almost always involve SWNTs grown directly or deposited on substrates with the most common substrate being SiO_2. Several studies have recently reported that the oxide substrate can have a strong influence on the observed Raman spectra with the most notable effect being the radial breathing mode (RBM) frequency variations.[38,39] O_2 adsorption effects may be facilitated, amplified, or entirely mediated by the substrate. In this paper, we examine the possible role of the oxide substrate with respect to O_2 adsorption induced variations especially on Raman *G*-band processes of individual metallic SWNTs. Comparisons between the part of a single nanotube that rests on the oxide substrate with the part of the same nanotube that is suspended over a trench patterned on the substrate are made. Increasing complexity of the *G*-band line shape and line narrowing upon continued annealing/O_2 adsorption cycle on both parts of the same metallic SWNT are observed. Strong correlation between D/G intensity ratio and the complexity of *G*-band features are also observed. Implications on the interpretation of Raman *G*-band features of metallic SWNTs are discussed.

II. EXPERIMENT

SWNTs were synthesized by chemical vapor deposition (CVD) using ferritin (Sigma-Aldrich) as catalyst on Si substrates with thermal oxide. SWNT growth was carried out at

900 °C with 300 cm^3/min of CH_4 and 100 cm^3/min of H_2 for on-substrate nanotubes. For the suspended SWNTs, CVD growth was carried out on Si/SiO_2 substrates with lithographically defined ~4 μm deep and ~10 μm wide trenches. Growth for suspended nanotubes was carried out at 925 °C with flow rates of 10 cm^3/min of CH_4 and 20 cm^3/min of H_2. The CVD growth step was always the last step of sample preparation to ensure that no postprocessing induced defects are present. SWNTs were placed in a controlled environment chamber with optical window and a heating stage for measurements. Annealing was carried out under continuous Ar flow (99.99% purity and ~20 cm^3/min flow rate) at 450 °C for 15 min unless indicated otherwise. Samples were cooled down in Ar to room temperature and kept under Ar flow for the Raman measurements (referred to as "Ar annealed"). For oxygen adsorption experiments, Raman measurements were carried out under continuous O_2 flow (99.99% purity and ~20 cm^3/min flow rate) at room temperature. Raman-scattering measurements were carried out with a JY LabRam HR 800 using 1.96 eV (633 nm) laser excitation source with a long working distance 100× air objective (laser spot diameter of ~1 μm). Laser power was kept at or below ~1 mW for all measurements.

III. RESULTS AND DISCUSSION

The *G*-band phonon modes of SWNTs derive from the in-plane E_{2g} modes of graphene. Symmetry considerations lead to six possible modes for *G*-band of SWNTs.[40] However, in single resonance Raman scattering with the experimental conditions used here, where the polarizations of the incident and detected light are both parallel to the nanotube orientation, only the totally symmetric A_1 modes are expected.[41–44] For armchair tubes, only the A_1^{TO} mode is then expected whereas only the A_1^{LO} mode is expected for zigzag tubes. For chiral nanotubes, both LO and TO modes may be observed. However, unlike these expectations, many, if not most, individual metallic SWNTs on substrates exhibit much more complex *G*-band spectra even in the parallel polarization/nanotube orientation configuration. This is exemplified in Fig. 1 lowermost spectrum where the *G*-band of the as-synthesized metallic nanotube measured in air is fitted with four peaks. These peaks are labeled P1–P4 with the lowest frequency P1 being the asymmetric Fano line and the rest being Lorentzians. The *D*-band peak at ~1320 cm^{-1} is also shown and is fitted with a single Lorentzian. This is the same fitting scheme used for all metallic tubes on substrate. In addition to the minimum four peaks observable for the *G*-band, this particular metallic tube, as well as many metallic tubes, exhibits relatively narrow linewidths and significantly upshifted *G*-band features.

Many of these observations about the individual metallic nanotubes' *G*-band features can be explained by Fermi-level shift induced by O_2 adsorption. When the Fermi level is near the Dirac point, softening and broadening of the LO mode are expected to arise from the Kohn anomaly.[30–35] Adsorption of O_2 shifts the Fermi level away from the Dirac point and the strong electron-phonon coupling is alleviated leading to upshifted and narrow *G*-band features. What the combination of O_2 induced Fermi-level shift and the phonon softening via Kohn anomaly cannot explain is the presence of more than two peaks (in most cases, described fairly well by four peaks) observed in the *G*-band Raman spectra of individual metallic tubes in the current experimental geometry. However, O_2 adsorption leads not only to a Fermi-level shift but also to an actual increase in the physical disorder and the enhanced disorder may be a key factor that complicates the *G*-band line shape. To elucidate the potential role of O_2 induced disorder, we examine how the Raman spectra of individual metallic SWNTs are altered by Ar annealing (O_2 desorption) and O_2 exposure cycles. First, measurements on metallic tubes on SiO_2 substrates are discussed. We then compare on-substrate and suspended segments of a single nanotube under Ar annealing/O_2 exposure cycles to sort out the possible role of the oxide substrate. In analyzing the Raman spectra, we consider the *G*-band LO mode linewidth decrease and stiffening as an indication of charge transfer shifting the Fermi level away from the Dirac point and the increasing D/G integrated intensity ratio as an indication of increasing physical disorder.

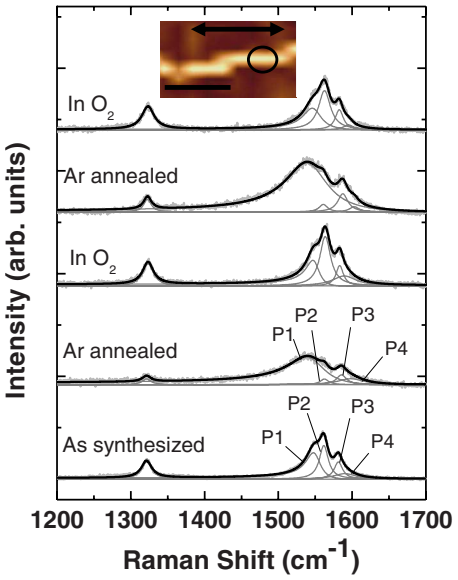

FIG. 1. (Color online) Raman spectra of *D*- and *G*-band regions of a single metallic nanotube under different conditions as indicated. Spectra are shown along with the curve fitting as described in the text. The second and the third spectra from the bottom correspond to the first Ar annealing/O_2 exposure cycle and the top two spectra to the second cycle. *G*-band Raman map of the nanotube is shown in the inset with the scale bar corresponding to 5 μm, double-headed arrow showing laser polarization, and the circle indicating the spot at which the spectra were obtained.

Figure 1 shows the Raman *G*-band map (inset) of a single metallic tube along with its *D*- and *G*-band spectra at different stages of Ar annealing/O_2 exposure cycle. As synthesized refers to the spectrum in air prior to any treatments. The CVD growth is the last step for sample preparation. Double-headed arrow in the Raman map indicates the laser polarization. Raman-scattered light is also detected in the same polarization. The circle indicates the spot at which the spectra were recorded. Based on RBM frequency of 190 cm^{-1}, we

tentatively assign this SWNT to a (12, 6) tube. If we assume single resonance process for the *G*-band, only the two totally symmetric A_1 modes should be observed for this chiral metallic tube in the given experimental condition. The *G*-band region contains three obvious features (P1–P3) of comparable intensities. Adding the fourth peak P4 leads to a much better fit but this peak usually has a relatively small intensity compared to the other peaks and less well defined. Therefore, we will limit our discussion to the three main peaks. Upon annealing under Ar (second spectrum from the bottom), there is a large broadening and softening of P1. The linewidth increases from 24 to 60 cm^{-1} and the peak position downshift from 1550 to 1545 cm^{-1}. The linewidth here refers to equivalent of full width at half maximum for the Fano line. Based on its being the broadest and the most softened of all *G*-band peaks and on its being the most dominant peak upon O_2 removal along with its peak position being closest to the expected value of ~1540 cm^{-1}, we assign P1 to the A_1^{LO} mode arising from single resonance Raman scattering. The broadening and softening of the A_1^{LO} mode upon Ar annealing are consistent with Fermi-level shift toward the Dirac point—i.e., adding electrons (or removing electron acceptors). The third spectrum from the top in Fig. 1 indicates that this charge-transfer effect arises mainly from adsorbed O_2. That is, upon exposure to O_2, the peak position and the width of A_1^{LO} mode as well as those of all other *G*-band peaks recover to similar values as the as-synthesized case measured in air. As shown in the top two spectra of Fig. 1, the Ar annealing/O_2 exposure cycle can be repeated and gives essentially the same results as the prior cycle with the exception of slight net increase in the *D*-band intensity in each cycle.

When the nanotube is annealed in Ar, P1 (the A_1^{LO} mode) and P3 become the two dominant features of the *G*-band. However, unlike the A_1^{LO} mode, P3 shows relatively small changes in the peak position throughout the Ar annealing/O_2 exposure cycles. Some tubes exhibit slightly larger P3 spectral shifts and even broadening. We suspect that the small shifts and broadening observed in P3 peak may be due to the unresolved P4 peak or another overlapping peak. However, the changes in P3 are always much smaller than those observed in the A_1^{LO} mode. Based on these observations (i.e., being one of the two dominant peaks when annealed and having little or no change with respect to O_2 adsorption/desorption) and its peak position being around 1580 cm^{-1}, we assign P3 to the single resonance A_1^{TO} mode. As will be discussed later, comparisons between on-substrate and suspended segments of a single nanotube further confirm this assignment.

Contrary to P1 and P3, P2 exhibits an opposite response with respect to its relative intensity change upon Ar annealing and O_2 exposure. In air, P2 is one of the most prominent peaks. After Ar annealing, it nearly disappears but reemerges as the dominant peak again upon O_2 exposure. These changes in P2 are directly correlated with the intensity changes in the *D*-band. Figure 2(a) shows how the Raman spectrum evolves over time as the nanotube is exposed to O_2 after Ar annealing. Relative *D*-band intensity (integrated D/G ratio) increase and progressive narrowing of *G*-band are observed. Highlighted in red is the P2 peak which exhib-

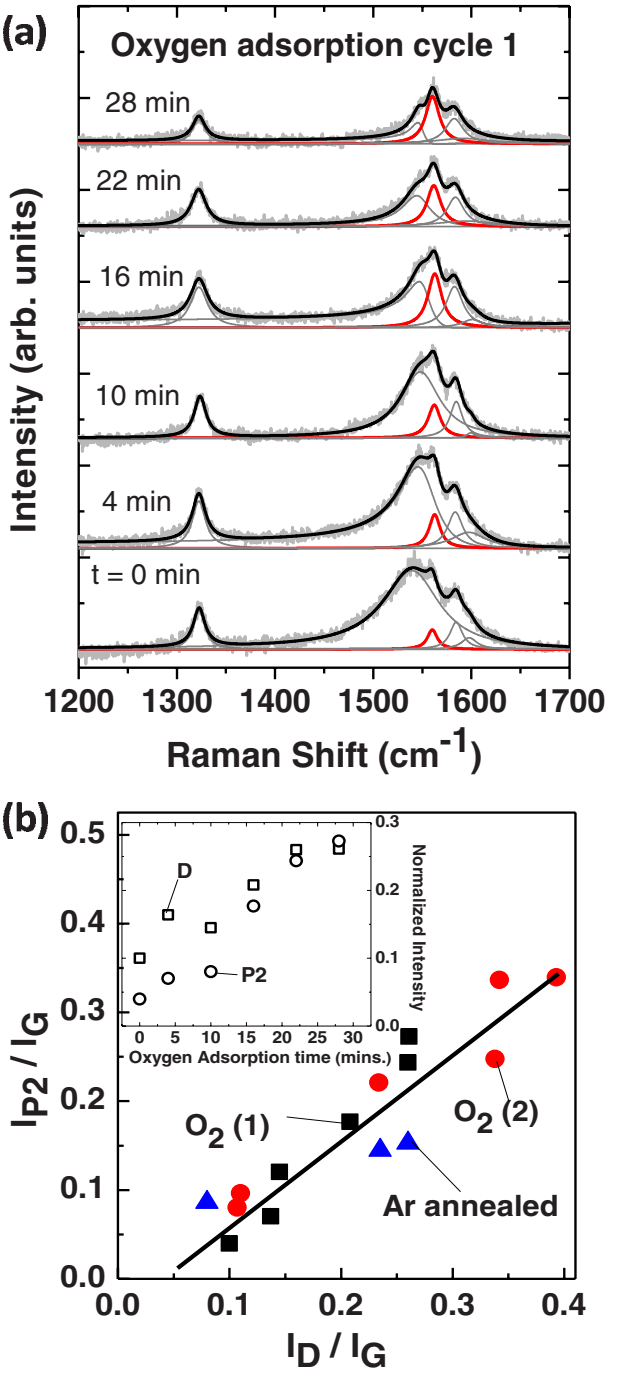

FIG. 2. (Color online) (a) Evolution of *D*- and *G*-band Raman spectra of the same metallic nanotube as in Fig. 1 at the indicated duration of O_2 exposure after Ar annealing and (b) the corresponding correlation between integrated P2 (highlight in red) and *D*-band intensities both normalized to the overall *G*-band integrated intensity. The blue triangles in (b) correspond to, from left to right, Ar annealing carried out at 450, 300, and 150 °C. For these three measurements, Ar annealing was carried out in steps from low to high temperatures with the sample continuously kept under Ar flow. After annealing at the given temperature, the sample was cooled to room temperature for the measurements then heated again to the next annealing temperature. Inset in (b) shows changes in the *D*-band (open squares) and P2 (open circles) integrated intensities normalized to the *G*-band intensity with O_2 exposure time.

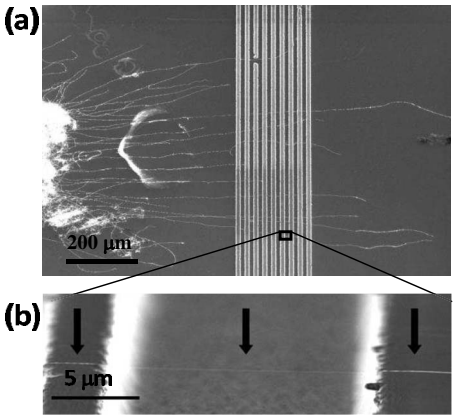

FIG. 3. (a) Scanning electron microscope image of nanotubes extending from the catalyst region on the left to lithographically patterned trenches and (b) an isolated suspended nanotube in the trench region at higher magnification. The arrows in (b) point to where the nanotube is located.

its increasing intensity with O_2 adsorption. The inset of Fig. 2(b) shows the changes in P2 and *D*-band intensities (both normalized to overall *G*-band intensity) over O_2 exposure time. The main panel plots normalized P2 intensity as a function of normalized *D*-band intensity. Results from two Ar anneal/O_2 exposure cycles are shown along with results from Ar annealing at different temperatures. Both P2 and *D*-band increase with increasing O_2 exposure time after Ar annealing. Higher annealing temperatures lead to larger decrease in both P2 and *D*-band. The linear dependence between P2 and *D*-band with a slope of 1 [indicated by the line shown in the main panel of Fig. 2(b)] strongly suggests that the observation of P2 peak is a direct consequence of physical disorder in the nanotube.

Keeping this direct linear relation between P2 and *D*-band intensities (and therefore the double-resonance process) in mind, we now compare and contrast on-substrate and suspended parts of a single nanotube in order to elucidate the complexity observed in *G*-band features of most metallic nanotubes. Figure 3(a) shows a scanning electron microscope image of several nanotubes suspended over a series of trenches. The bright area on the left side of the trenches corresponds to the catalyst area. Raman measurements are carried out in the trench regions far away from the catalyst. Figure 3(b) shows a typical isolated single nanotube suspended over a trench on which Raman spectra are obtained.

Figure 4(a) shows the *G*-band Raman intensity map for a suspended metallic nanotube. The double-headed arrow corresponds to the incident laser polarization which is also same as the polarization of the detected light. The brighter background regions on the left and right ends of the map correspond to the oxide substrate and the suspended part of the nanotube is over the darker background. Based on the RBM frequency of 195 cm^{-1} for the suspended part and the on-substrate RBM frequency of 197 cm^{-1} [Fig. 4(b)], we tentatively assign this nanotube to (13, 4) chiral nanotube. Figures 4(c) and 4(d) show *D*- and *G*-band spectral regions for the on-substrate and the suspended segments of this nanotube as synthesized (bottommost spectra).

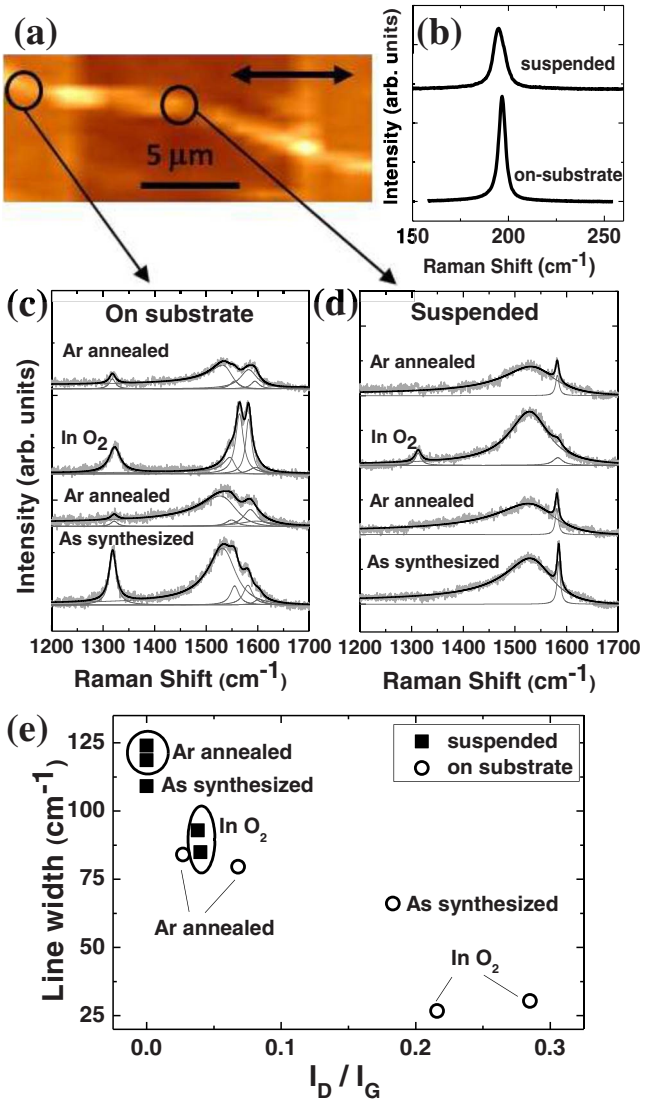

FIG. 4. (Color online) (a) *G*-band Raman map of a suspended metallic nanotube, (b) RBM spectra of suspended and on-substrate parts of the nanotube as synthesized, *D*- and *G*-band spectra of the same tube under different conditions as indicated for (c) the on-substrate and (d) the suspended parts, and (e) change in the A_1^{LO} linewidth with D/G integrated intensity ratio. Double arrow in the *G*-band map indicates the laser polarization.

There are two obvious and striking differences between the on-substrate and the suspended parts of the nanotube. First, the *G*-band of the on-substrate part is rather complex with four or more features whereas the *G*-band of the suspended part can be described very well with only two peaks [see bottom fitted spectra of Figs. 4(c) and 4(d)]. We note that Zhang *et al.*[38] also observed very similar spectral differences between suspended and on-substrate parts of a single nanotube but they have not elaborated on the differences. The two-peak *G*-band of the suspended part is what is expected for the chiral metallic tube under single resonance condition with current experimental configuration. The lower frequency broad and asymmetric Fano line corresponds to the softened A_1^{LO} phonon. The higher narrow Lorentzian corresponds to the A_1^{TO} mode. Peak positions of 1540 and

1584 cm^{-1} further confirm these assignments for the suspended part. The second salient difference is in the *D*-band being observed only in the on-substrate region. The complex *G*-band features observed only in the on-substrate segment are consistent with the direct relation between P2, an unexpected peak based on single resonance process, and the degree of disorder we have shown in Fig. 2. These differences imply large degree of O_2 adsorption induced electron removal and physical disorder when the nanotube rests on an oxide substrate. Suspended part of the tube is essentially free of these O_2 induced effects. These observations are also consistent with what has been observed in semiconducting tubes where scanning probe gate measurements have shown on-substrate segment to be *p* doped while the suspended part remains intrinsic.[45]

Although at first glance, the responses of the on-substrate and suspended parts of this nanotube to Ar annealing/O_2 exposure cycle appear different, both can be explained by the same O_2 adsorption effects of charge transfer and induced disorder. The on-substrate part starts out with relatively broad and softened *G*-band compared to the nanotube in Fig. 1 but its response to Ar annealing/O_2 exposure cycle is qualitatively the same as in Fig. 1. It is consistent with what is expected from removal and introduction of O_2 induced charge transfer and disorder (i.e., broadening and softening of A_1^{LO} mode and decrease in the *D*-band intensity upon annealing and the opposite changes upon O_2 adsorption). The suspended part of the nanotube, on the other hand, shows only very small changes upon annealing. Since the *G*-band already appears very broadened and softened and the *D*-band is not present to begin with, we expect little or no O_2 induced charge transfer and disorder that can be undone by Ar annealing. There is a slight broadening of the A_1^{LO} mode indicating that O_2 adsorption effects may be present but not enough to cause any noticeable *D*-band intensities. However, when this annealed tube is exposed to O_2, the *D*-band intensity becomes non-negligible. The width of the A_1^{LO} mode Fano line decreases and upshifts slightly as well. Figure 4(e) shows that the changes in the A_1^{LO} mode linewidth of the suspended region extrapolate well to that of the on-substrate part. That is, whether the metallic nanotube rests on the oxide substrate or not, O_2 adsorption can induce both disorder and charge transfer. Furthermore, these results suggest that the O_2 adsorption needs to be activated (e.g., by heating) to observe significant effects when the nanotube is freestanding. Much more pronounced and readily observed changes for the on-substrate part of the nanotube indicate that both the charge transfer and disorder introduction are facilitated by the oxide substrate. A possible reason for enhanced O_2 induced charge transfer and disorder may be that the immediate substrate surface sites (e.g., defect sites) catalytically activate O_2 into a more reactive form. Further studies are needed to elucidate atomic details of how the substrate enhances these effects.

In addition to the slight narrowing and upshifting of its *G*-band A_1^{LO} peak and the appearance of the *D*-band, the suspended part of the nanotube exhibits much less distinct A_1^{TO} peak upon postannealing O_2 exposure. With the reduced A_1^{TO} intensity, the Raman spectrum of the suspended part begins to appear similar to that of the on-substrate section

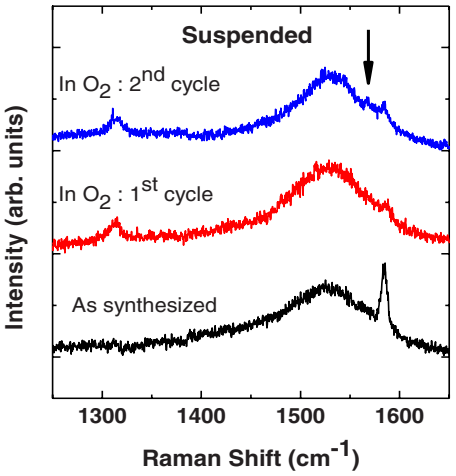

FIG. 5. (Color online) Raman *D*- and *G*-band spectra from suspended part of the nanotube in Fig. 4 as synthesized and after O_2 exposure. Each O_2 exposure is carried out after Ar annealing at 450 °C. The arrow points to the appearance of additional peak in the second O_2 adsorption cycle.

(after Ar annealing). Figure 5 shows that second Ar annealing step followed by O_2 adsorption continues to change the *G*-band features especially in regions around the A_1^{TO} mode. The arrow in Fig. 5 indicates what appears to be a new peak showing up in the spectral region between the A_1^{LO} and the A_1^{TO} mode peak positions—i.e., analogous to the P2 peak in Fig. 1. This increasing complexity (i.e., appearance or enhancement of P2) in the *G*-band spectrum concurrent with disorder increase is observed in all metallic nanotubes (12 on substrate and 2 suspended) that we have measured.

Given the fixed experimental geometry, the appearance of new peaks or the enhancement of peaks other than the A_1^{LO} and A_1^{TO} modes (e.g., the P2 peak) in the *G*-band of metallic tubes cannot arise from variations in the polarization with respect to nanotube orientation allowing E_1 and E_2 modes to be observable. Symmetry breaking by the substrate causing complexity in the *G*-band can also be ruled out based on the appearance of additional peaks upon continued Ar annealing/O_2 adsorption cycle in the suspended segment of the nanotube. Then, given the strong and linear dependence (with a slope of 1) of P2 intensity on the degree of disorder [Fig. 2(b)], we suggest that the peaks other than A_1^{LO} and A_1^{TO} modes observed in the *G*-band arise from the double-resonance process[46] much like the *D*-band. Although single resonance has been shown to be the dominant *G*-band process,[47] double-resonance scattering is expected to become more significant with increasing disorder.[48] The second resonance is more likely in metallic tubes than in semiconducting ones given the continuous finite density of states. The increasing disorder also provides increasing probability of momentum-conserving elastic scattering by defects. Hence, in metallic tubes resting on SiO_2 substrates (or freestanding but with heat activated O_2 adsorption), the Raman *G*-band spectra become complex due to the presence of both single and double-resonance modes with the latter arising from O_2 induced disorder.

IV. CONCLUSIONS

We have shown that metallic tubes free from ambient O_2 adsorption induced effects show simple single resonance *G*-band spectral profile dominated by totally symmetric A_1 modes. We have pointed out three consequences of O_2 adsorption on the Raman spectra of metallic tubes: (1) introduction of disorder and therefore an increase in the *D*-band intensity, (2) narrowing and stiffening of *G*-band A_1^{LO} mode via charge-transfer induced Fermi-level shift, and (3) the appearance of double-resonance modes complicating *G*-band spectra. By comparing spectral responses of on-substrate and suspended regions of the same nanotube to annealing/O_2 exposure cycles, we have shown that the substrate enhances these O_2 adsorption effects. However, the substrate is not solely responsible for the observed complexity in the *G*-band features since the same effects can result from heat activated adsorption of O_2 on the freestanding segments of nanotubes. These results have several important implications on our understanding of fundamental processes in metallic nanotubes. For example, polarization dependence of metallic tube Raman *G*-band scattering will need to be re-examined in light of double-resonance processes if more than two peaks are observed in the experimental configuration where the incident and scattered light polarizations are both parallel to nanotube orientation. With respect to experimental verification of Kohn anomaly induced phonon softening, we suspect that the varying degree of softening and broadening observed in the A_1^{LO} mode and sometimes in what appears to be the A_1^{TO} mode with Fermi-level shift[29,35] are due to the presence of double-resonance features complicating the Raman spectra.

ACKNOWLEDGMENTS

This material is based upon work supported by NSF (Grants No. DMR-0348585 and No. CCF-0506660).

*Corresponding author; mshim@illinois.edu

[1] P. T. Araujo, S. K. Doorn, S. Kilina, S. Tretiak, E. Einarsson, S. Maruyama, H. Chacham, M. A. Pimenta, and A. Jorio, Phys. Rev. Lett. **98**, 067401 (2007).
[2] J. Maultzsch, H. Telg, S. Reich, and C. Thomsen, Phys. Rev. B **72**, 205438 (2005).
[3] A. Jorio, R. Saito, J. H. Hafner, C. M. Lieber, M. Hunter, T. McClure, G. Dresselhaus, and M. S. Dresselhaus, Phys. Rev. Lett. **86**, 1118 (2001).
[4] A. M. Rao, J. Chen, E. Richter, U. Schlecht, P. C. Eklund, R. C. Haddon, U. D. Venkateswaran, Y. K. Kwon, and D. Tomanek, Phys. Rev. Lett. **86**, 3895 (2001).
[5] J.-C. Charlier, P. C. Eklund, J. Zhu, and A. C. Ferrari, Top. Appl. Phys. **111**, 673 (2008).
[6] A. Z. Hartman, M. Jouzi, R. L. Barnett, and J. M. Xu, Phys. Rev. Lett. **92**, 236804 (2004).
[7] M. Oron-Carl, F. Hennrich, M. M. Kappes, H. v. Lohneysen, and R. Krupke, Nano Lett. **5**, 1761 (2005).
[8] J. Maultzsch, S. Reich, and C. Thomsen, Phys. Rev. B **65**, 233402 (2002).
[9] A. G. Souza Filho, A. Jorio, G. G. Samsonidze, G. Dresselhaus, R. Saito, and M. S. Dresselhaus, Nanotechnology **14**, 1130 (2003).
[10] C. Wang, Q. Cao, T. Ozel, A. Gaur, J. A. Rogers, and M. Shim, J. Am. Chem. Soc. **127**, 11460 (2005).
[11] K. H. An, J. S. Park, C.-M. Yang, S. Y. Jeong, S. C. Lim, C. Kang, J.-H. Son, M. S. Jeong, and Y. H. Lee, J. Am. Chem. Soc. **127**, 5196 (2005).
[12] K. Kamaras, M. E. Itkis, H. Hu, B. Zhao, and R. C. Haddon, Science **301**, 1501 (2003).
[13] D. Chattopadhyay, I. Galeska, and F. Papadimitrakopoulos, J. Am. Chem. Soc. **125**, 3370 (2003).
[14] M. S. Strano, C. A. Dyke, M. L. Usrey, P. W. Barone, M. J. Allen, H. Shah, C. Kittrell, R. H. Hauge, J. M. Tour, and R. E. Smalley, Science **301**, 1519 (2003).
[15] M. Shim, T. Ozel, A. Gaur, and C. J. Wang, J. Am. Chem. Soc. **128**, 7522 (2006).
[16] L. Kavan and L. Dunsch, Nano Lett. **3**, 969 (2003).
[17] S. Kazaoui, N. Minami, N. Mastuda, H. Kataura, and Y. Achiba, Appl. Phys. Lett. **78**, 3433 (2001).
[18] L. Kavan, P. Rapta, L. Dunsch, M. J. Bronikowski, P. Willis, and R. E. Smalley, J. Phys. Chem. B **105**, 10764 (2001).
[19] A. M. Rao, P. C. Eklund, S. Bandow, A. Thess, and R. E. Smalley, Nature (London) **388**, 257 (1997).
[20] G. U. Sumanasekera, C. K. W. Adu, S. Fang, and P. C. Eklund, Phys. Rev. Lett. **85**, 1096 (2000).
[21] S.-H. Jhi, S. G. Louie, and M. L. Cohen, Phys. Rev. Lett. **85**, 1710 (2000).
[22] P. G. Collins, K. Bradley, M. Ishigami, and A. Zettl, Science **287**, 1801 (2000).
[23] S. Heinze, J. Tersoff, R. Martel, V. Derycke, J. Appenzeller, and Ph. Avouris, Phys. Rev. Lett. **89**, 106801 (2002).
[24] M. Shim and G. P. Siddons, Appl. Phys. Lett. **83**, 3564 (2003).
[25] G. Dukovic, B. E. White, Z. Zhou, F. Wang, S. Jockusch, M. L. Steigerwald, T. F. Heinz, Ri. A. Friesner, N. J. Turro, and L. E. Brus, J. Am. Chem. Soc. **126**, 15269 (2004).
[26] M. Shim, J. H. Back, T. Ozel, and K.-W. Kwon, Phys. Rev. B **71**, 205411 (2005).
[27] D. Kang, N. Park, J. Hyun, E. Bae, J. Ko, J. Kim, and W. Park, Appl. Phys. Lett. **86**, 093105 (2005).
[28] V. Barone, J. Heyd, and G. E. Scuseria, Chem. Phys. Lett. **389**, 289 (2004).
[29] K. T. Nguyen, A. Gaur, and M. Shim, Phys. Rev. Lett. **98**, 145504 (2007).
[30] S. Piscanec, M. Lazzeri, F. Mauri, A. C. Ferrari, and J. Robertson, Phys. Rev. Lett. **93**, 185503 (2004).
[31] M. Lazzeri, S. Piscanec, F. Mauri, A. C. Ferrari, and J. Robertson, Phys. Rev. B **73**, 155426 (2006).
[32] S. Piscanec, M. Lazzeri, J. Robertson, A. C. Ferrari, and F. Mauri, Phys. Rev. B **75**, 035427 (2007).
[33] N. Caudal, A. M. Saitta, M. Lazzeri, and F. Mauri, Phys. Rev. B **75**, 115423 (2007).
[34] Y. Wu, J. Maultzsch, E. Knoesel, B. Chandra, M. Huang, M. Y. Sfeir, L. E. Brus, J. Hone, and T. F. Heinz, Phys. Rev. Lett. **99**,

027402 (2007).
[35] H. Farhat, H. Son, Ge. G. Samsonidze, S. Reich, M. S. Dresselhaus, and J. Kong, Phys. Rev. Lett. **99**, 145506 (2007).
[36] C. Jiang, K. Kempa, J. Zhao, U. Schlecht, U. Kolb, T. Basché, M. Burghard, and A. Mews, Phys. Rev. B **66**, 161404(R) (2002).
[37] M. Paillet, Ph. Poncharal, A. Zahab, J.-L. Sauvajol, J. C. Meyer, and S. Roth, Phys. Rev. Lett. **94**, 237401 (2005).
[38] Y. Zhang, H. Son, J. Zhang, M. S. Dresselhaus, J. Kong, and Z. Liu, J. Phys. Chem. C **111**, 1983 (2007).
[39] Y. Zhang, J. Zhang, H. Son, J. Kong, and Z. Liu, J. Am. Chem. Soc. **127**, 17156 (2005).
[40] R. Saito, G. Dresselhaus, and M. S. Dresselhaus, *Physical Properties of Carbon Nanotubes* (Imperial College, London, 2003).
[41] R. Saito, A. Jorio, J. H. Hafner, C. M. Lieber, M. Hunter, T. McClure, G. Dresselhaus, and M. S. Dresselhaus, Phys. Rev. B **64**, 085312 (2001).
[42] A. Jorio, M. A. Pimenta, A. G. Souza Filho, G. G. Samsonidze, A. K. Swan, M. S. Ünlü, B. B. Goldberg, R. Saito, G. Dresselhaus, and M. S. Dresselhaus, Phys. Rev. Lett. **90**, 107403 (2003).
[43] C. Thomsen, S. Reich, and J. Maultzsch, Philos. Trans. R. Soc. London, Ser. A **362**, 2337 (2004).
[44] Z. Yu and L. E. Brus, J. Phys. Chem. B **105**, 1123 (2001).
[45] E. Minot, Y. Yaish, V. Sazonova, and P. L. McEuen, Nature (London) **428**, 536 (2004).
[46] C. Thomsen and S. Reich, Phys. Rev. Lett. **85**, 5214 (2000).
[47] M. Souza, A. Jorio, C. Fantini, B. R. A. Neves, M. A. Pimenta, R. Saito, A. Ismach, E. Joselevich, V. W. Brar, G. G. Samsonidze, G. Dresselhaus, and M. S. Dresselhaus, Phys. Rev. B **69**, 241403(R) (2004).
[48] J. Maultzsch, S. Reich, U. Schlecht, and C. Thomsen, Phys. Rev. Lett. **91**, 087402 (2003).